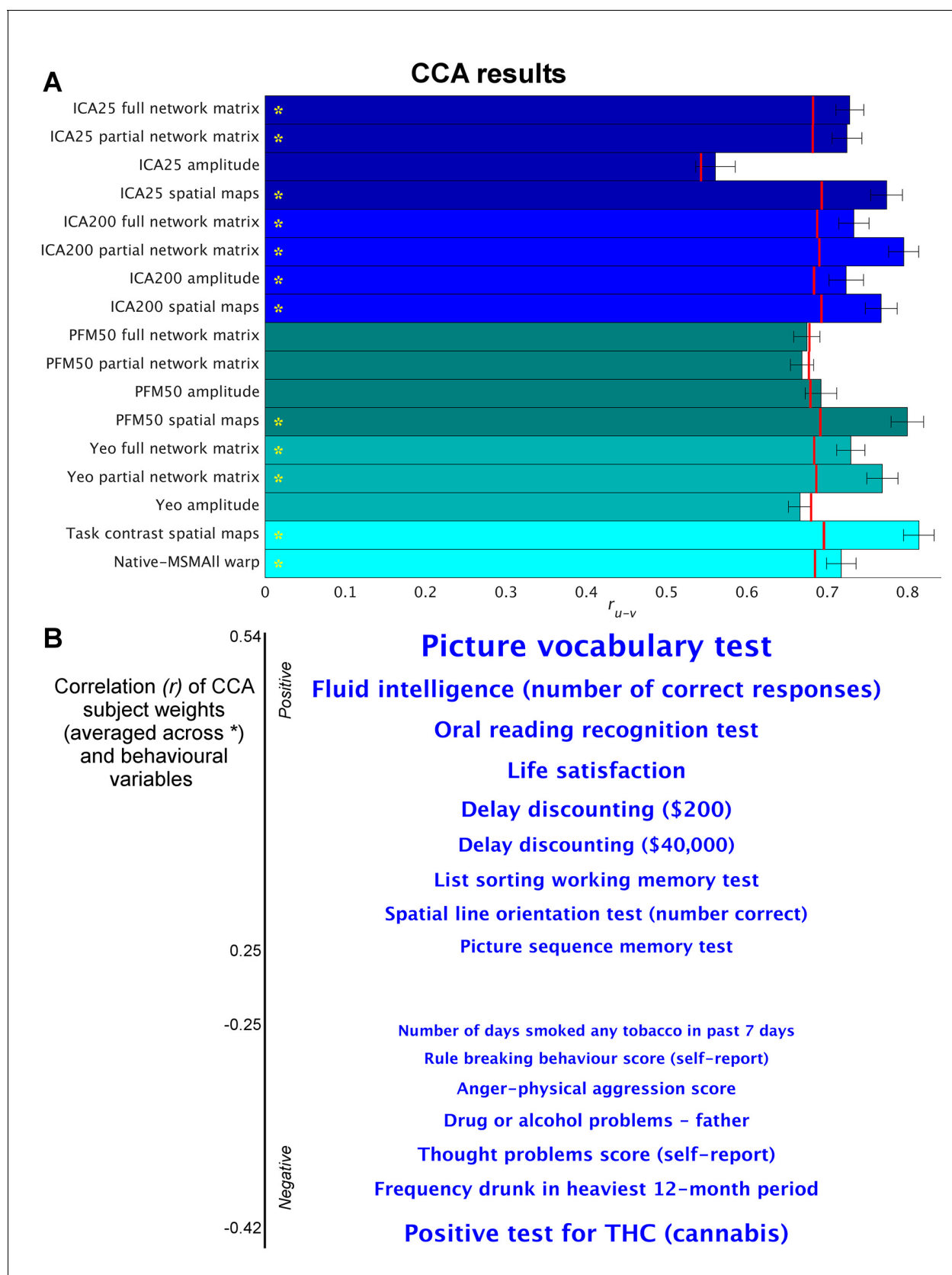# Figures and figure supplements

The relationship between spatial configuration and functional connectivity of brain regions

Janine Diane Bijsterbosch *et al*

**Figure 1.** Highly similar associations between behaviour and the brain occur across 17 distinct measures derived from fMRI. (**A**) Comparison of strength of CCA result for network matrices, spatial maps and amplitudes (node timeseries standard deviation) derived from several distinct group-average
Figure 1 continued on next page

Figure 1 continued

spatial parcellations/decompositions: ICA decompositions at two scales of detail (dimensionalities of 25 and 200, with 'ICA200 partial network matrix' corresponding to the measures used previously [*Smith et al., 2015*]); a PROFUMO decomposition (PFM; dimensionality 50); an atlas-based hard parcellation (108 parcels [*Yeo et al., 2011*]), task contrast spatial maps (86 contrasts, 47 unique), and warp field from native space to MSMAll alignment. Each bar reports a separate CCA analysis (first CCA mode shown), performed against behaviour/life-factors. A similar mode of variation is found across most of the parcellation methods and different fMRI measures. r_{UV} is the strength of the canonical correlation between imaging and non-imaging measures. Error bars indicate confidence intervals (2.5–97.5%) estimated using surrogate data (generated with the same correlation structure), and red lines reflect the p<0.002 significant threshold compared with a null distribution obtained with permutation testing (i.e. family-wise-error corrected across all CCA components and Bonferroni corrected across a total of 25 CCAs performed, see *Supplementary file 1a and b* for the full set of results). CCA estimates the highest possible r_{uv} given the dataset; therefore, the null distribution for low-dimensional brain data (e.g. ICA 25 amplitude) is expected to be lower than for high-dimensional brain data. (**B**) Set of non-imaging variables that correlate most strongly with the CCA mode (averaged subject weights V across results marked with * in A; i.e. p=0.00001) with behavioural variables. Position against the y-axis and font size indicate strength of correlation.

DOI: https://doi.org/10.7554/eLife.32992.003
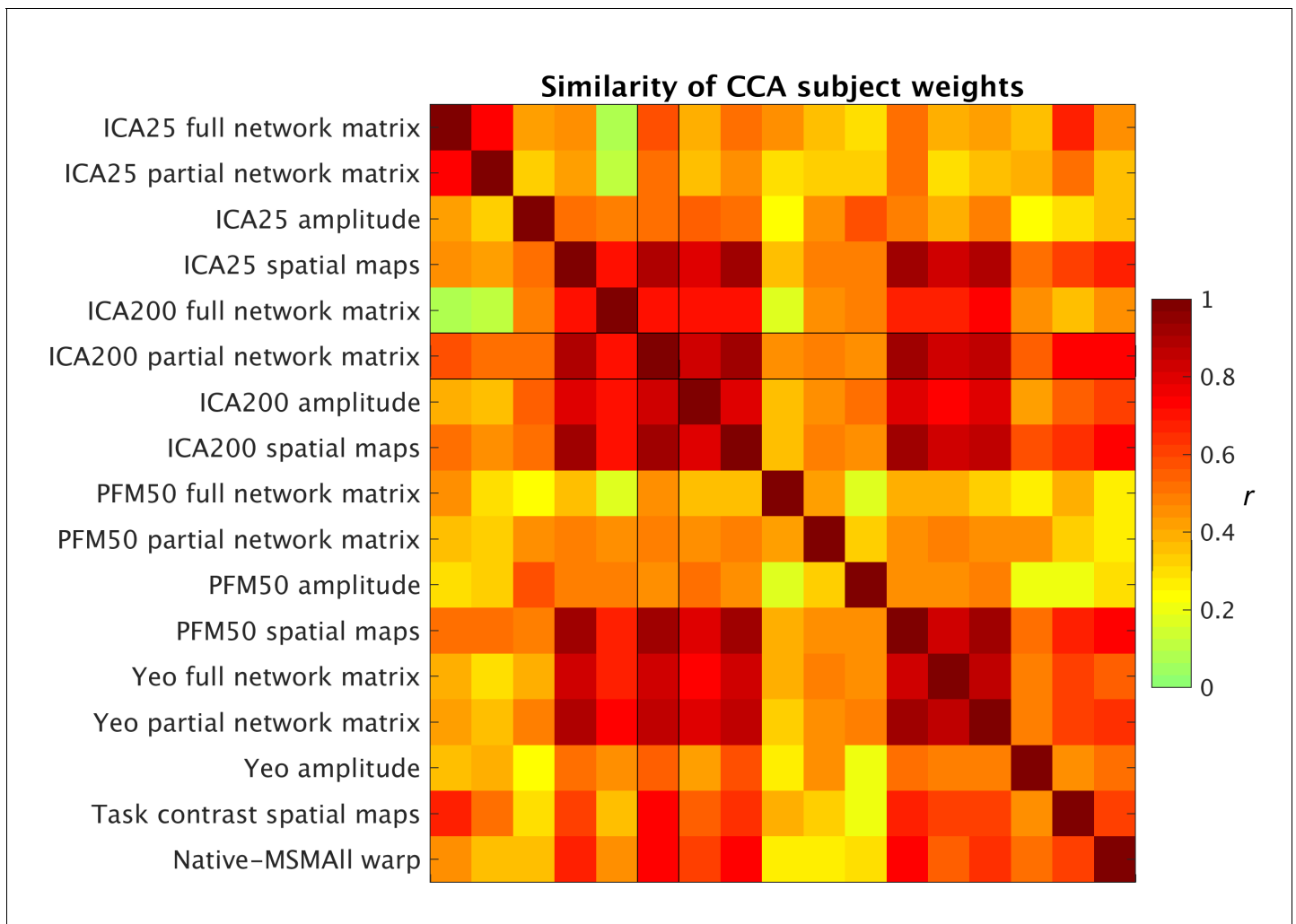
Figure 1—figure supplement 1. Similarity of behavioural subject weights from a range of separate CCA analyses between MRI-derived measures and behavioural measures. For each CCA instance, the mode with the maximum correlation with the ICA200 partial network matrix was selected for comparison. Absolute correlation values between behavioural subject weights (V) are shown and reveal that a comparable behavioural mode is obtained from the CCAs.

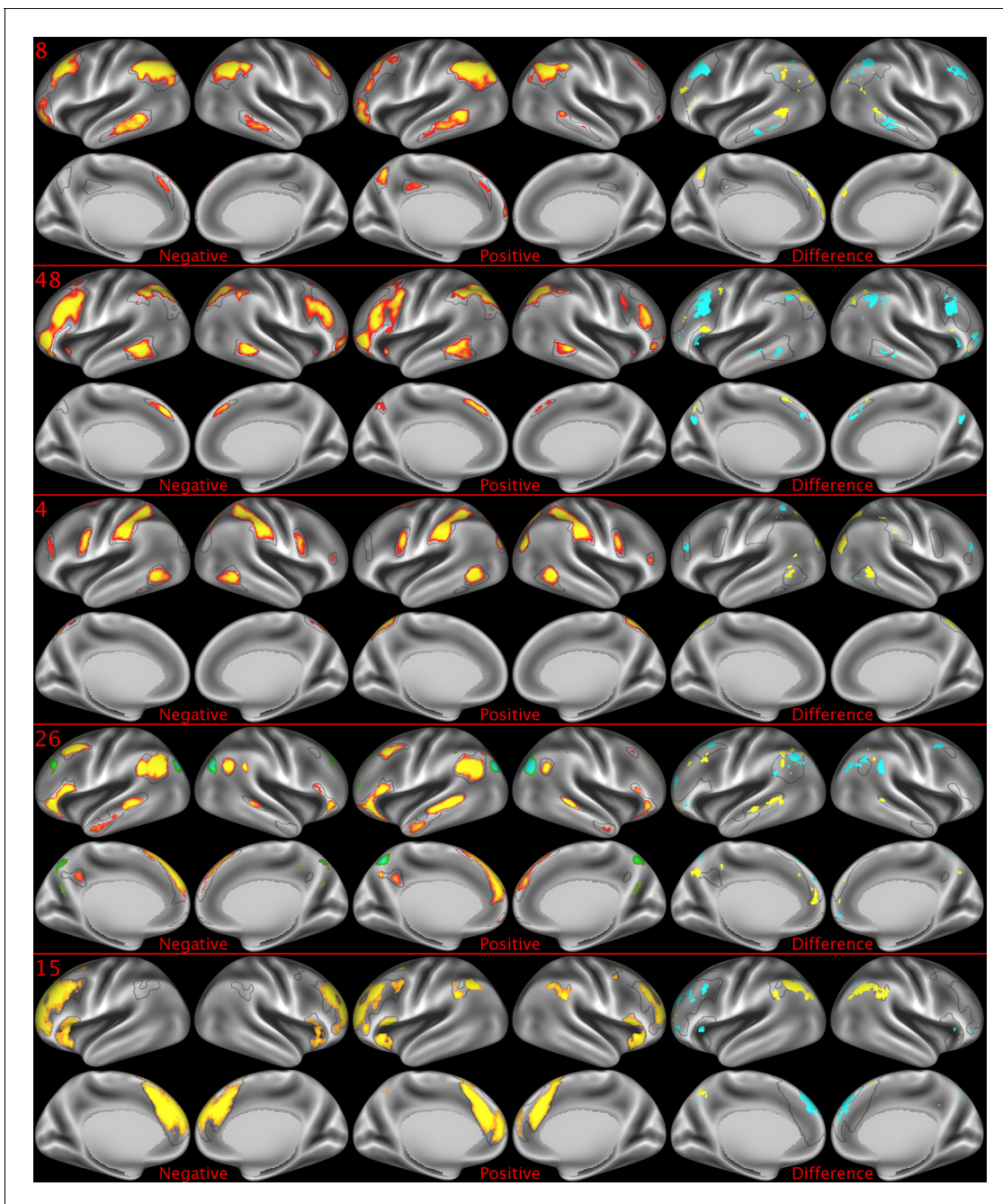DOI: https://doi.org/10.7554/eLife.32992.005
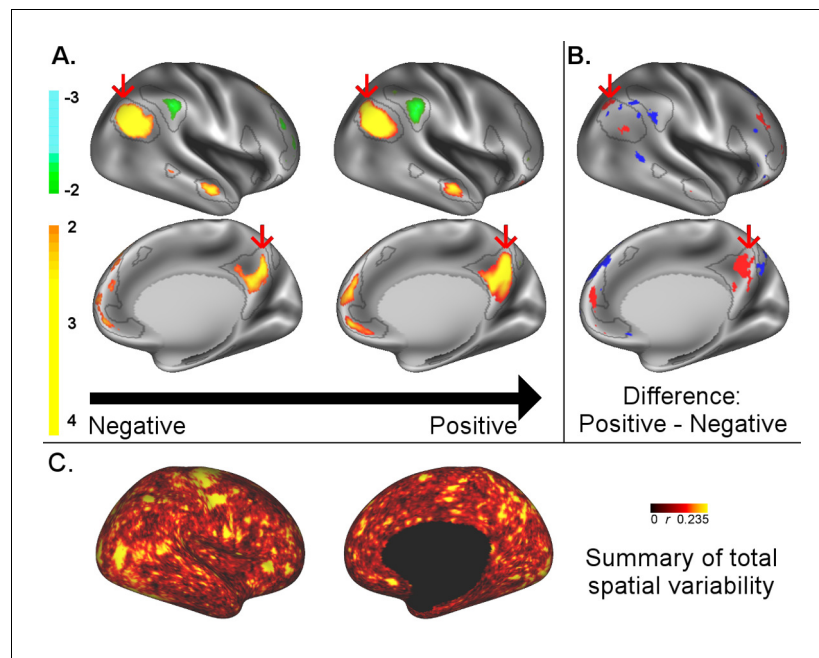
Figure 2. A: representative maps of the two extreme ends (identified based on the low and high extremes along a linearly spaced vector that spans the full range of subject CCA scores) of the CCA mode of population covariation continuum are shown for the default mode network (DMN, the PFM mode that contributed most strongly to the CCA mode of population covariation). The top row shows that the inferior parietal node of the DMN differs in shape and extends into the intraparietal sulcus in subjects who score high on the positive-negative CCA mode (right), compared with subjects who score lower (left). The bottom row shows that medial prefrontal and posterior cingulate/precuneus regions of the DMN differ in size and shape as a function of the CCA positive-negative mode. The representative maps at both extremes are thresholded at ±2 (arbitrary units specific to the PFM algorithm) for visualisation purposes (the differences are not affected by the thresholding; for unthresholded video-versions of these maps, please see the Supplementary video files. The grey contours are identical on the left and right to aid visual comparison and are based on the group-average maps (thresholded at 0.75). Spatial changes of all PFM modes can be seen in the Supplementary video files and in *Figure 2—figure supplements 2–7*. B: difference maps (positive - negative; thresholded at ±1) are shown to aid comparison. C: A summary of topographic variability across all PFM modes, showing PFM correlations with CCA subject weights (at each grayordinate the maximum absolute r across all PFMs is displayed). An extended version of C is available in *Figure 2—figure supplement 7*. Data of *Figure 2* available at: https://balsa.wustl.edu/8lVx.
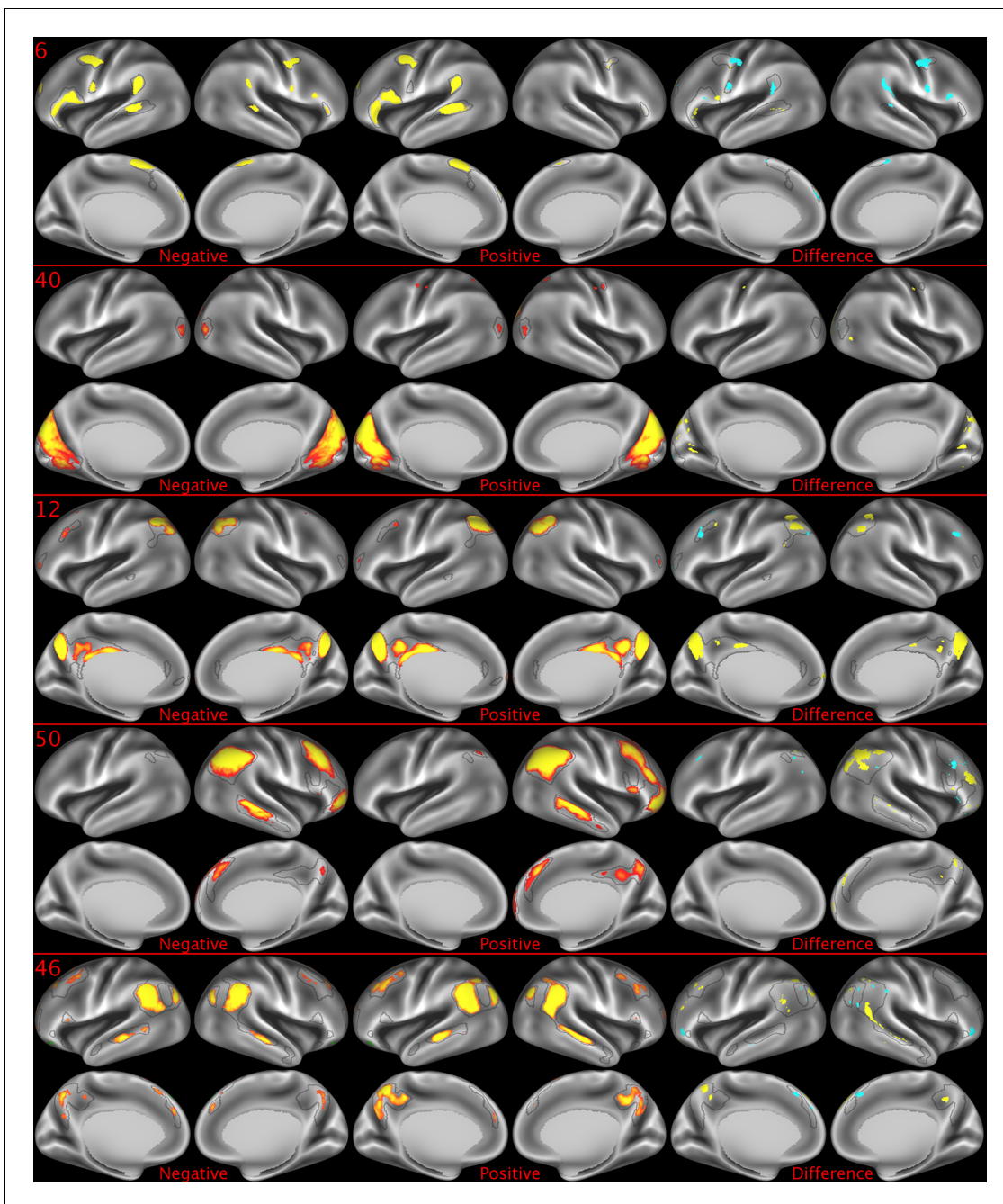DOI: https://doi.org/10.7554/eLife.32992.006
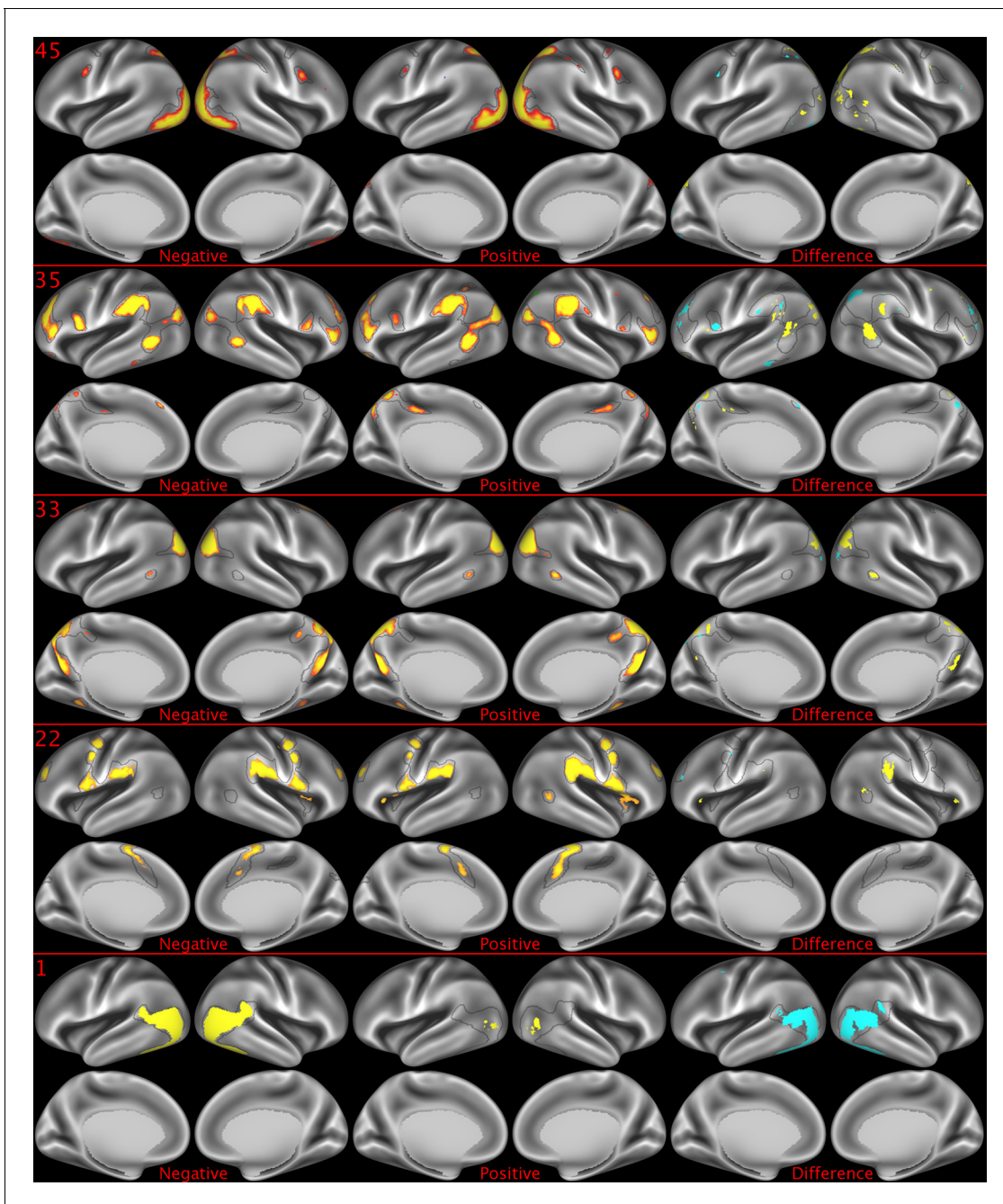
Figure 2—figure supplement 1. Representative maps of the two extreme ends of the positive-negative continuum for five PFMs. Maps can directly be compared between the left (negative) and the middle (positive), and difference maps are shown on the right (blue = negative > positive; yellow = positive > negative). Arbitrary thresholds used for visualisation purposes (same thresholds for all maps), see videos for the unthresholded continuum. Gray outlines are based on group average maps and are identical between left and right images to facilitate comparison. Data available at https://balsa.wustl.edu/07pz, https://balsa.wustl.edu/21kq, https://balsa.wustl.edu/rKMN, https://balsa.wustl.edu/xK16, https://balsa.wustl.edu/PGw5.

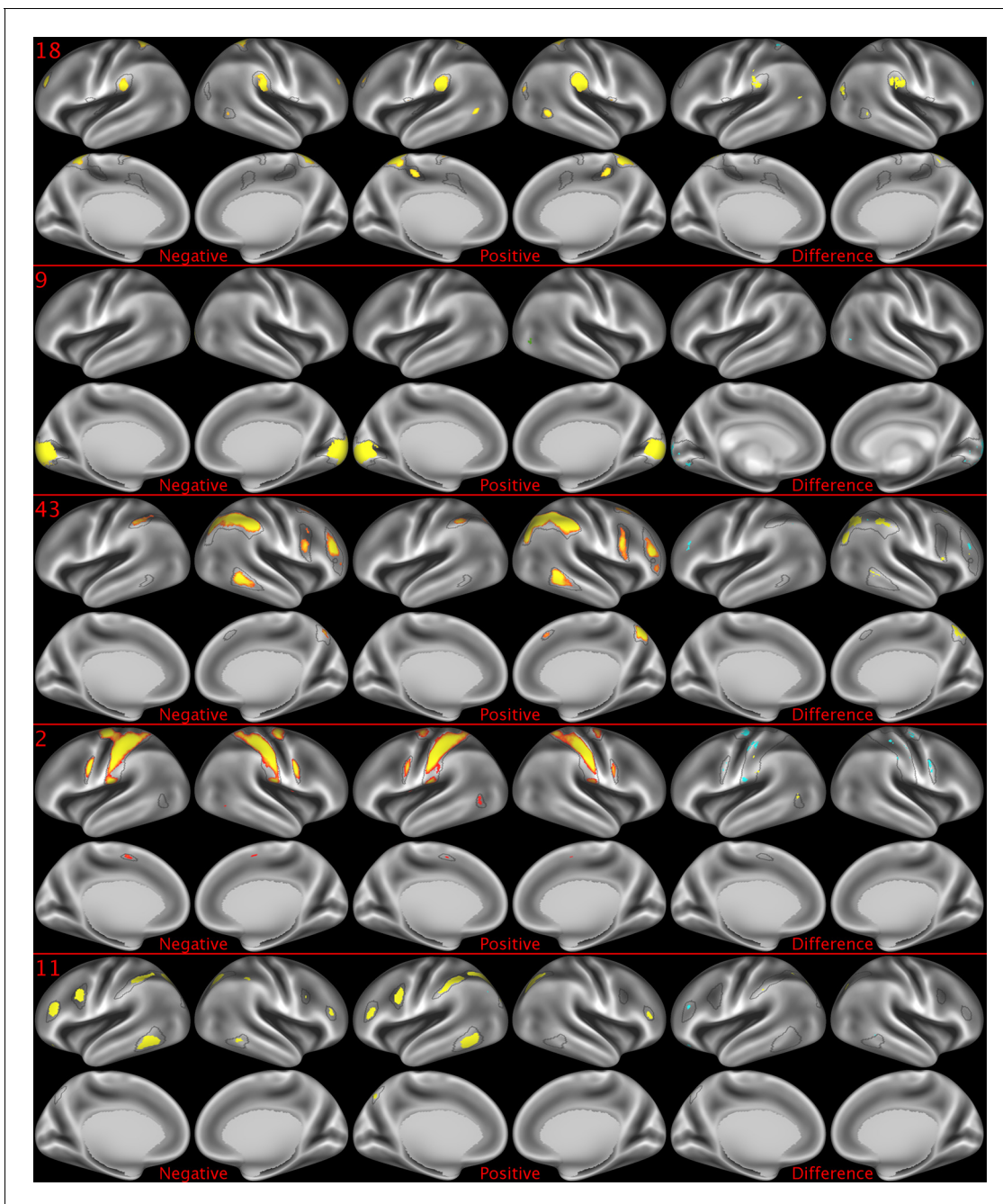DOI: https://doi.org/10.7554/eLife.32992.007

Figure 2—figure supplement 2. Representative maps of the two extreme ends of the positive-negative continuum for five PFMs. Maps can directly be compared between the left (negative) and the middle (positive), and difference maps are shown on the right (blue = negative > positive; yellow = positive > negative). Arbitrary thresholds used for visualisation purposes (same thresholds for all maps except map 15, where lower thresholds were used), see videos for the unthresholded continuum. Gray outlines are based on group average maps and are identical between left and right images to facilitate comparison. Data available at https://balsa.wustl.edu/KMGg, https://balsa.wustl.edu/Nq9K, https://balsa.wustl.edu/G1mN, https://balsa.wustl.edu/LBLx, https://balsa.wustl.edu/pKwg.
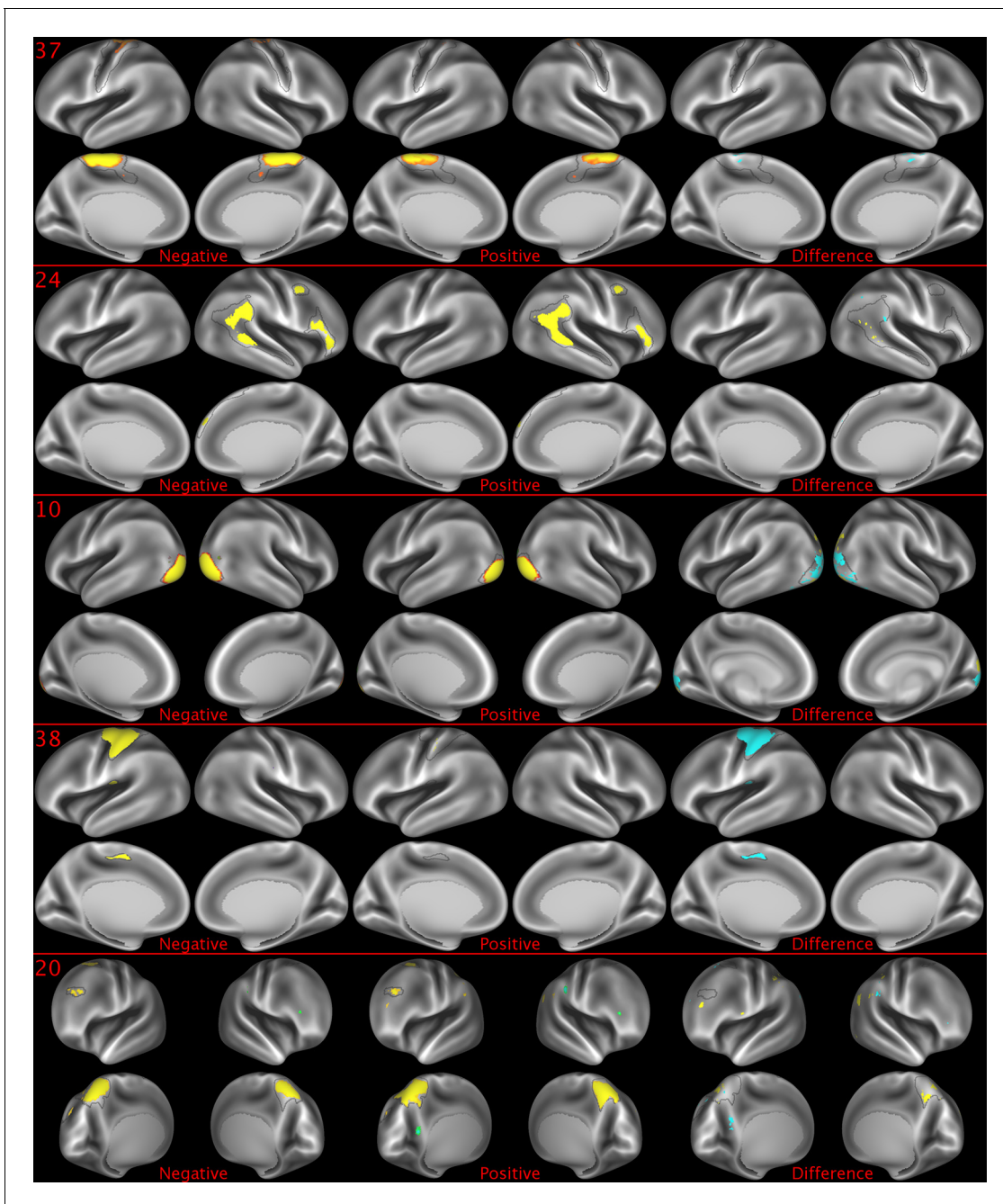DOI: https://doi.org/10.7554/eLife.32992.008

Figure 2—figure supplement 3. Representative maps of the two extreme ends of the positive-negative continuum for five PFMs. Maps can directly be compared between the left (negative) and the middle (positive), and difference maps are shown on the right (blue = negative > positive; yellow = positive > negative). Arbitrary thresholds used for visualisation purposes (same thresholds for all maps), see videos for the unthresholded continuum. Gray outlines are based on group average maps and are identical between left and right images to facilitate comparison. Data available at https://balsa.wustl.edu/9qw5, https://balsa.wustl.edu/kKxK, https://balsa.wustl.edu/07m9, https:// balsa.wustl.edu/21gB, https://balsa.wustl.edu/rKw9.
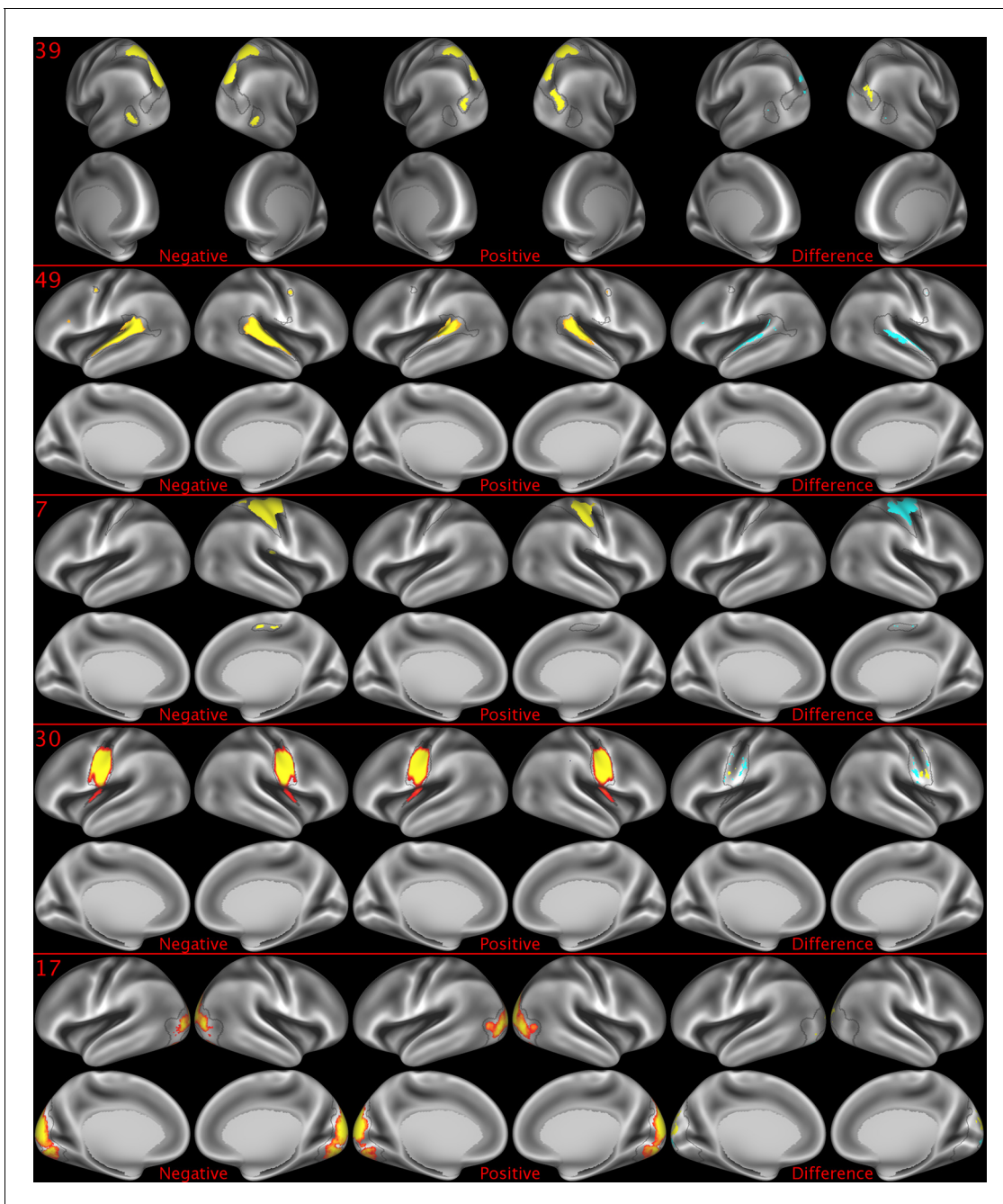DOI: https://doi.org/10.7554/eLife.32992.009

Figure 2—figure supplement 4. Representative maps of the two extreme ends of the positive-negative continuum for five PFMs. Maps can directly be compared between the left (negative) and the middle (positive), and difference maps are shown on the right (blue = negative > positive; yellow = positive > negative). Arbitrary thresholds used for visualisation purposes (same thresholds for all maps), see videos for the unthresholded continuum. Gray outlines are based on group average maps and are identical between left and right images to facilitate comparison. Data available at https://balsa.wustl.edu/xKwn, https://balsa.wustl.edu/PG0X, https://balsa.wustl.edu/7B1G, https://balsa.wustl.edu/6M1K, https://balsa.wustl.edu/16mg.
DOI: https://doi.org/10.7554/eLife.32992.010

Figure 2—figure supplement 5. Representative maps of the two extreme ends of the positive-negative continuum for five PFMs. Maps can directly be compared between the left (negative) and the middle (positive), and difference maps are shown on the right (blue = negative > positive; yellow = positive > negative). Arbitrary thresholds used for visualisation purposes (same thresholds for all maps except map 20, where lower thresholds were used), see videos for the unthresholded continuum. Gray outlines are based on group average maps and are identical between left and right images to facilitate comparison. Data available at https://balsa.wustl.edu/5g1G, https://balsa.wustl.edu/nKVP, https://balsa.wustl.edu/gKkP, https://balsa.wustl.edu/Mlpw, https://balsa.wustl.edu/Brql.
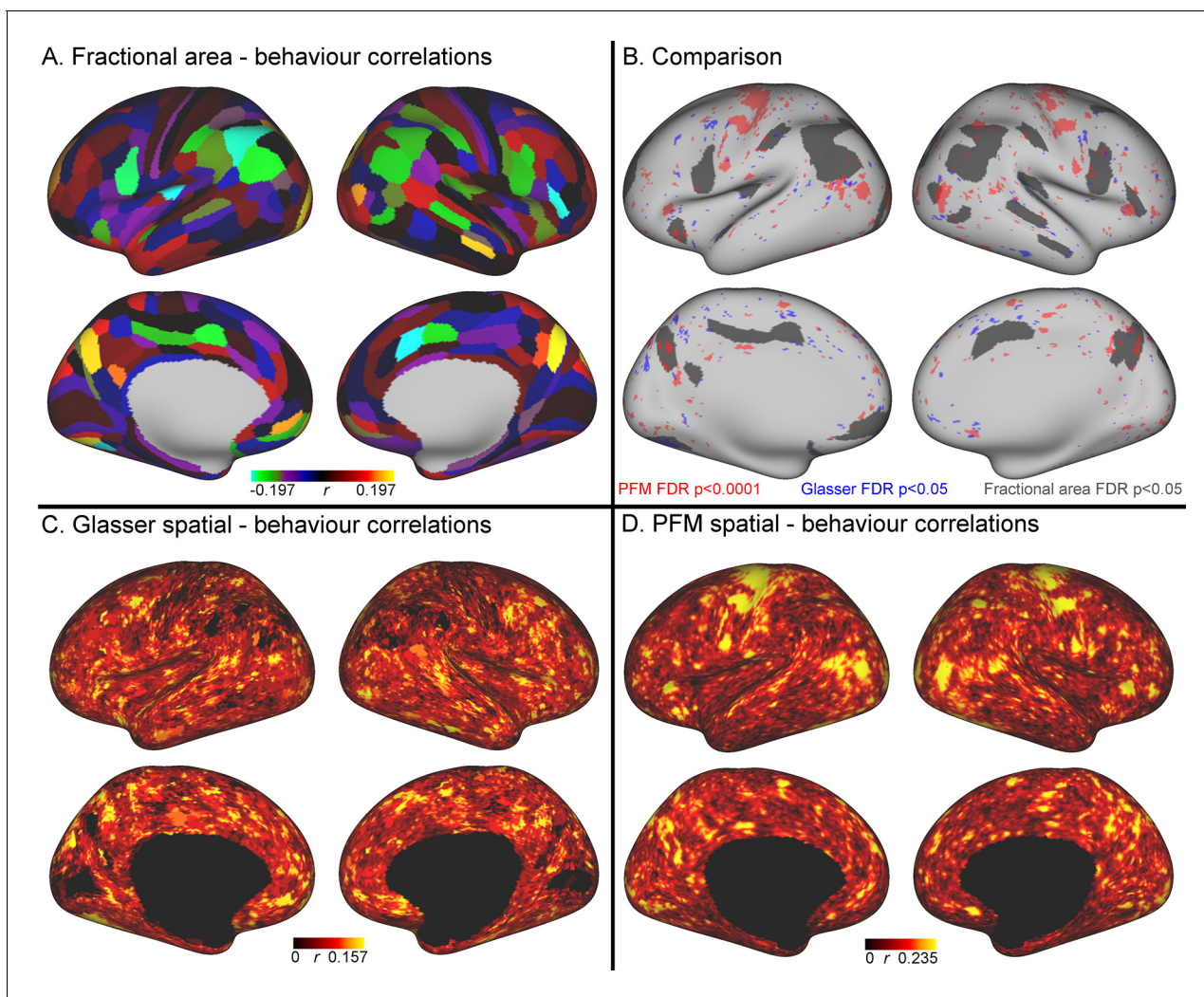
DOI: https://doi.org/10.7554/eLife.32992.011

Figure 2—figure supplement 6. Representative maps of the two extreme ends of the positive-negative continuum for five PFMs. Maps can directly be compared between the left (negative) and the middle (positive), and difference maps are shown on the right (blue = negative > positive; yellow = positive > negative). Arbitrary thresholds used for visualisation purposes (same thresholds for all maps), see videos for the unthresholded continuum. Gray outlines are based on group average maps and are identical between left and right images to facilitate comparison. Data available at https://balsa.wustl.edu/lK0L, https://balsa.wustl.edu/qK7x, https://balsa.wustl.edu/jK9z, https://balsa.wustl.edu/wKjp, https://balsa.wustl.edu/4nL6.
DOI: https://doi.org/10.7554/eLife.32992.012

Figure 2—figure supplement 7. Comparison of the cortical representation of associations with behaviour across fractional area, HCP_MMP1.0 individual subject parcellation and PFM spatial maps. (**A**) Correlations between fractional area and behaviour were highly consistent between left and right hemispheres, and revealed relatively high correlations in higher order sensory and cognitive regions. Specifically, bilaterally significant (FDR corrected p<0.05) positive associations between larger surface area and higher scores on the positive-negative mode of population covariation were found in area POS2 of the parieto-occipital sulcus and in area IPS1 of the dorsal visual processing stream; bilaterally significant negative correlations were identified in the cingulate motor area 24dv, premotor area 6 r, and inferior parietal cortex (areas PFt, PFm, PGi). (**B**) Qualitative comparison between the spatial localisation of strongest correlations with behaviour across all three datasets reveals that many regions that contribute strongly in either the HCP_MMP1.0 or in the PFM individual subject spatial estimates spatially overlap or adjoin cortical areas in which fractional surface area was also closely linked to behaviour. This qualitative finding suggests that differences in regional surface area may drive many of the results presented in this work, although further research is needed to confirm this interpretation (for visual comparison the PFM correlation maps are shown using a higher threshold p_{FDR} <0.0001, $|r|$ > 0.218, and HCP_MMP1.0 correlation maps are correlated at p_{FDR} <0.05; $|r|$ > 0.159). (**C**) Un-thresholded HCP_MMP1.0 correlations with CCA subject weights; these are the maximum absolute r across all parcels, and therefore do not contain the parcel structure itself. (**D**) Un-thresholded PFM correlations with CCA subject weights (maximum absolute r across all PFMs). The cortical localisation of strong associations with behaviour do not closely overlap between PFMs and the HCP_MMP1.0 parcellation (i.e. red and blue regions in B and un-thresholded maps in C/D). This lack of exact correspondence of the representations of cross-subject variability may reflect differences between the HCP_MMP1.0 and PROFUMO models (the former being a hard parcellation with no overlap between parcels, and the latter being a soft parcellation that includes complex and often overlapping networks), and differences in the data types driving the parcellation (PROFUMO being driven by rfMRI data only, and the HCP_MMP1.0 parcellation being driven by data from multiple different modalities). Data available at https://balsa.wustl.edu/mK28.

DOI: https://doi.org/10.7554/eLife.32992.013
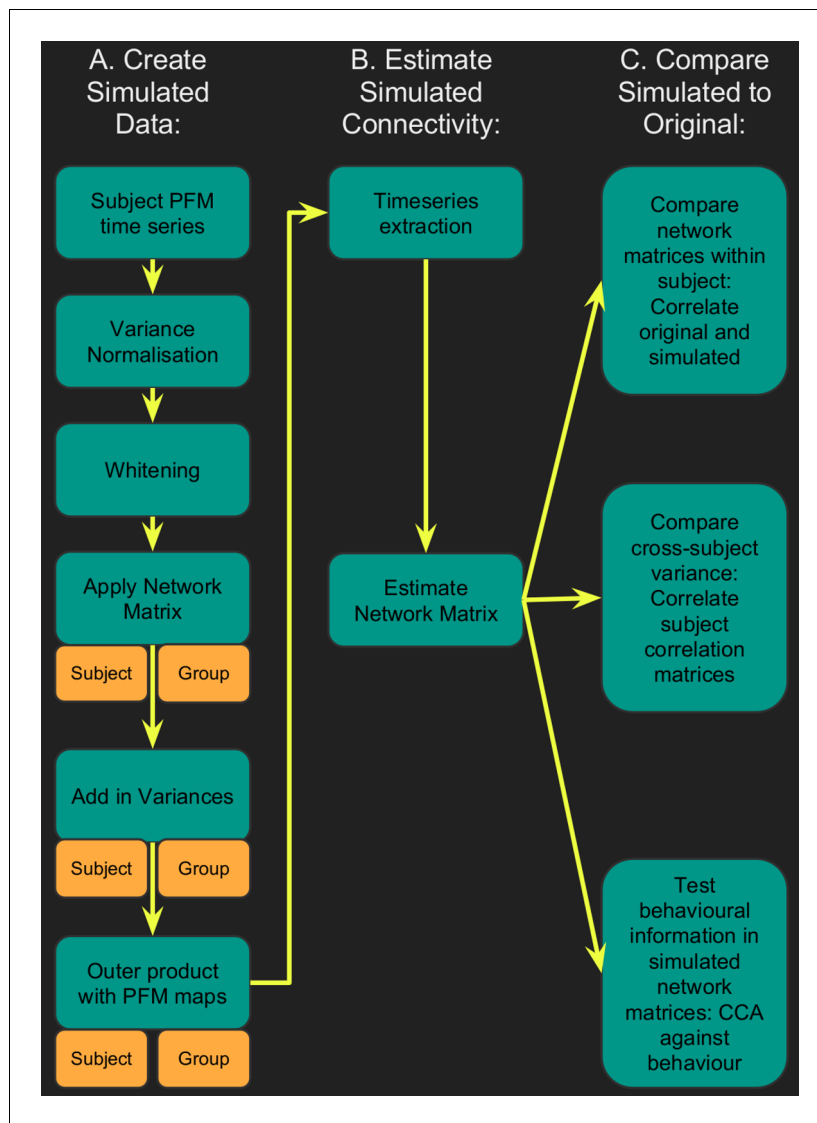
Figure 3. Flowchart for spatiotemporal simulations. Simulated data was generated for each subject by setting one or more aspects (from the network matrices, node amplitudes, and spatial maps) to the group average. Timeseries extraction is performed (uinsg either dual regression against original group ICA maps, or masked against a binary parcellation); network matrices are calculated and compared against network matrices estimated from the original data.

DOI: https://doi.org/10.7554/eLife.32992.023
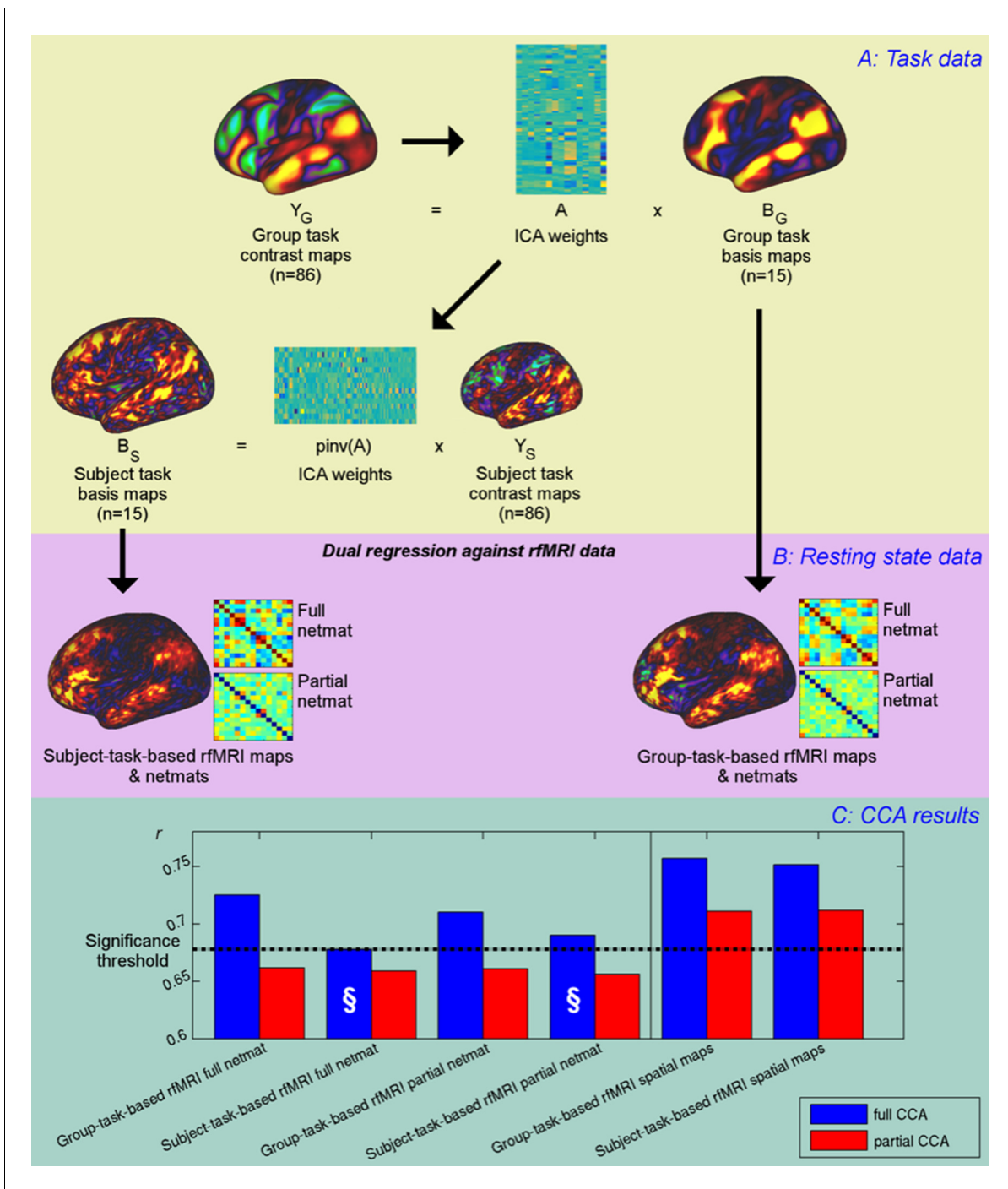
Figure 4. Unique contribution of topography versus coupling. (**A**) Task basis maps are extracted from group-averaged task contrasts (n=86, 47 unique) using ICA to ensure correspondence of basis maps across subjects. These maps represent the basic building blocks of any activation pattern, and subject task basis maps (obtained by applying the ICA weights to subject task contrast maps) are not influenced by misalignment problems. (**B**) Dual regression against rfMRI data is performed using either the (potentially misaligned) group task basis maps or the (functionally localised) subject task basis maps. (**C**) CCA results of group-task-based rfMRI maps and network matrices and of subject-task-based rfMRI maps and netmats. The results show rUV (i.e., the correlation between the first U and V obtained from the CCA analysis describing the strength of association between the rfMRI and behavioural measures). The null line (i.e., p=0.05 based on permutation testing) is shown as a dotted line at 0.68; results below this line do not reach significance. The blue bars show the main CCA results using the complete data, and the red bars show partial CCA results computed after regressing out any variance that can be explained by network matrices from the spatial maps and vice versa prior to running the CCA. The results show a general decrease in rUV for all measures when comparing partial to full CCA results. The strongest partial CCA result (red bars on right) are found when using

Figure 4 continued

rfMRI spatial maps, and the associated netmats showed the weakest results ("§"). However, the partial CCA results for the spatial maps (i.e., the red bars on the right) still reach significance. All of the partial CCAs also showed lower rU-Uica compared to the full CCAs (not shown here).
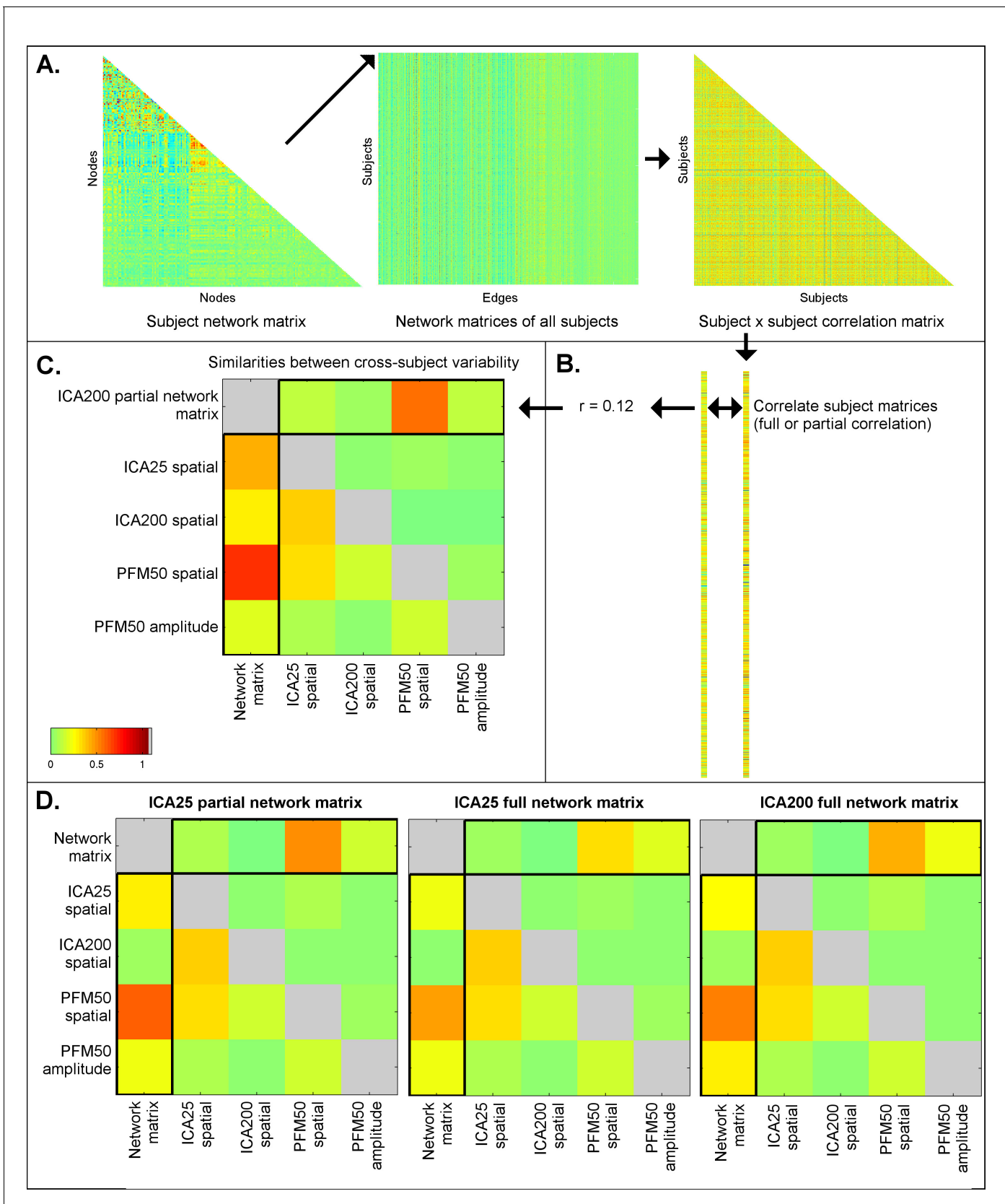
Figure 4—figure supplement 1. Similarities between cross-subject variations estimated from different rfMRI measures. Subject-by-subject correlation matrices are estimated (**A**), and vectorised (**B**; one subject correlation matrix being estimated for each measure type). The first column of the similarities

Figure 4—figure supplement 1 continued

(C; highlighted) shows the relationship (full correlation) between the ICA network matrix and various other measures, such as PFM spatial maps and amplitudes, and ICA spatial maps. These results show that the ICA network matrix is closely related to PFM spatial maps. The first row of the similarities (C; highlighted) shows the same relationship after taking into account all the other elements (i.e. the partial correlation between different measures). This reveals that PFM spatial maps are strongly linked to the ICA network matrix, even after accounting for any variance that can be explained by ICA spatial maps and PFM amplitudes. Similar results are obtained for ICA 200 and 25 dimensionality and for partial and full network matrices (D). These findings are consistent with the simulation results in *Table 1*, showing that estimated network matrices and spatial topography to a large extent overlap in terms of the interesting cross-subject variability they represent. Additionally, the results show that while dual regression ICA spatial maps are able to capture some of the subject spatial variability, subject maps estimated by PROFUMO capture considerably more spatial variability over and above the dual regression maps.